Lattice bow in thick, homoepitaxial GaN layers for vertical power devices

Qiang Liu [a,*], Naoki Fujimoto [b], Jian Shen [b,c], Shugo Nitta [b], Atsushi Tanaka [b,d], Yoshio Honda [b], Zlatko Sitar [b,e], Michał Boćkowski [b,f,] Yoshinao Kumagai [b,g], and Hiroshi Amano [a,b,h,i]

[a] Graduate School of Engineering, Nagoya University, Nagoya, 464-8603, Japan

[b] Institute of Materials and Systems for Sustainability, Nagoya University, Nagoya, 464-8601, Japan

[c] School of Chemistry and Chemical Engineering, Harbin Institute of Technology, Harbin 150001, China.

[d] National Institute for Materials Science, Tsukuba, 305-0044, Japan

[e] Department of Materials Science and Engineering, North Carolina State University, Raleigh, NC 27695, USA

[f] Institute of High Pressure Physics, Polish Academy of Sciences, Sokolowska 29/37, 01-142 Warsaw, Poland

[g] Department of Applied Chemistry, Tokyo University of Agriculture and Technology, Koganei, Tokyo 184-8588, Japan

[h] Akasaki Research Center, Nagoya University, Nagoya, 464-8603, Japan

[i] Venture Business Laboratory, Nagoya University, Nagoya, 464-8603, Japan

Keywords: A1. Lattice bow; A3. Thick GaN homoepitaxy; B1. Nitrides; B2. Semiconducting III-V materials; B3. Vertical power devices;

Abstract

Lattice bow generated by 40 µm thick HVPE homoepitaxial layers on commercial free-standing, ammonothermal and HVPE GaN wafers was studied. While a change in lattice bow was measured for all wafers, the additional bow on the ammonothermal GaN wafers was minimal. The main driving force for the observed increase in the lattice bow for HVPE wafers was related to stress in the films generated by the elongation of dislocations via climb and generation of new dislocations at the homoepitaxial interface. Lattice bow is a crucial wafer parameter as it determines the variation of the offcut across

the surface. If an offcut variation of 0.1° is allowed for desired control surface morphology, composition of alloys, and uniformity of doping on this surface, the measured bow on the two HVPE GaN wafers and one ammonothermal GaN wafer limits their uniformity-diameter to ~0.5", 1" and >4", respectively.

1. Introduction

Power rectifiers and switches working at high currents and breakdown voltages are sought-after for the realization of efficient power transmission within the context of smart grids and transformation of “green energy”. They will have broad applications for electric motor drives, power converters, solar cell inverters, energy storage, and energy transmission. It is projected that by 2030 as much as 80% of the electricity generated will pass through one or more power conversion stage from generation to consumption [1]. Maximizing the energy efficiency of switching semiconductor devices in these power conversion stages is, therefore, of utmost importance. GaN-based high power switches are being developed as the building blocks of future low loss power grids [2]. Current pathways to develop GaN-based high power devices are focused on either GaN Schottky diodes [3] or p-n junction-based JFETs [4] or CAVETs [5], [6].

All proposed GaN power devices incorporate a free-standing GaN substrate and a relatively thick n^- GaN drift layer, usually grown by halide vapor phase epitaxy (HVPE) [5],[7],[8],[9]. To achieve uniform growth and doping across the entire wafer, which is paramount for achieving high reliability and high yield, a tight control of the surface offcut is required for all device layers, usually within 0.1° [10]. Even though the starting substrate may meet these requirements, the homoepitaxial growth of thick n^- drift layers may induce additional stress and lattice bow due to a difference in point defect concentration, dislocation density, or dislocation bending.

In this study, the effect of 40 µm thick layers (representing the growth of thick drift layers for vertical devices) on the final state of the HVPE overgrowth were studied on various commercial, free-standing GaN substrates in terms of dislocation density and lattice bow.

2. Experimental procedures

2.1. Growth apparatus

The HVPE-GaN layers were grown in a vertical, atmospheric-pressure HVPE reactor. The Ga metal in the source zone was heated resistively and the temperature was controlled by a thermocouple in contact with the quartz reactor wall. Herein, liquid Ga reacted with HCl to form GaCl. The growth zone, where GaN crystal growth occurred, was heated by RF power coupled into a cylindrical graphite susceptor. The temperature of the graphite substrate holder was controlled by a thermocouple placed in the center of the holder about 10 mm below the surface. A pyrometer with a spot size of ~10 mm was used to monitor the surface temperature of the center of the rotating wafer during growth.

The process gases entered the reactor through the top inlets and were exhausted at the bottom. They were injected into the growth zone through three concentric nozzles: GaCl was supplied through the center nozzle, N_2 flowing through the middle nozzle was used as a separation gas to delay the reaction between the Ga and nitrogen species and to prevent parasitic deposition on the injection nozzles, while NH_3 was injected through the outermost nozzle. Deposition on the inner quartz reactor wall was minimized by an N_2 curtain gas flow.

2.2. Samples

Commercially available 2-inch ammonothermal (Sample A) and HVPE (Samples B and C) GaN (0001) wafers were chosen for this study to cover a range of initial dislocation densities, lattice bows, and doping conditions. All wafers were n-type and the pertinent wafer parameters are listed in Table I. All growth studies were performed on 8x8 mm^2 squares diced from the commercial 2-inch wafers.

Table I. Various initial GaN wafer parameters; all wafers were 2 inch in diameter and n-type.

	Growth method	Electron density [cm^{-3}]	RMS roughness [nm]	Offcut/ direction [deg]	Thickness [μm]	Dislocation density [cm^{-2}]
Sample A	Ammonothermal	$< 10^{19}$	< 0.5	0.3/[1$\bar{1}$00]	500	$< 5\times10^{4}$
Sample B	HVPE	$\sim10^{19}$	< 0.35	0.3/[1$\bar{1}$00]	356	7.9×10^{5}
Sample C	HVPE	1.3×10^{18}	< 0.35	0.5/[11$\bar{2}$0]	415	4.6×10^{6}

2.3. Growth procedures

During the growth process, the temperatures of the source and growth zones were kept constant at 750ºC and 1050ºC, respectively. The input V/III ratio of 30 was achieved with HCl and NH_3 flow rates of 13 and 390 sccm, respectively. The carrier gas for GaCl was a nitrogen-hydrogen mixture (660 sccm) consisting of 1 part nitrogen and 2 parts hydrogen; N_2 (2.9 slm) was used as NH_3 diluent, separation gas (5 slm), and curtain gas (7.8 slm). The growth process lasted for 1 hour in this study.

Prior to growth, both the source and growth zones were preheated in the nitrogen atmosphere to 500ºC. At this point, ammonia flow was initiated and heating to the final temperatures of the two zones continued at 12.5ºC/min and 25ºC/min, respectively. When the desired temperatures were reached, hydrogen and HCl flows were initiated and the crystallization process began. After a thickness of 40 μm was reached, the flow to the Ga source was switched off and the growth zone was cooled down at 20ºC/min in ammonia atmosphere until a temperature of 400ºC was reached.

2.4. Sample characterization

X-ray diffraction (XRD) measurements were carried out prior and after the growth using a Philips X'Pert Pro materials research diffractometer. Rocking curves of the symmetric (0002) and asymmetric $(10\bar{1}2)$ reflections were recorded with a four-bounce Ge (220) symmetrical monochromator before the sample to evaluate the tilt and twist, respectively.

Lattice bow, measured as the radius of curvature, R_C, was evaluated using seven (0002) rocking curves taken along the orthogonal $[1\bar{1}00]$ and $[11\bar{2}0]$ directions at an interval of 1 mm, similar to the method described in Ref. [11]. The beam size was 0.3 mm × 3 mm with the longer dimension perpendicular to the diffraction plane.

The dislocations in the substrates and epilayers were analyzed using two-photon excitation photoluminescence (2PPL) [12]. The method allowed for a direct visualization of dislocations as a function of the depth in the sample. The dislocation inclination angle, α, in the epi-layers was calculated from the 3D dislocation model built from 50 × 50 μm^2

2PPL slices taken at 1 μm depth intervals. The direction of the inclination and the inclination angle were calculated from the x-y coordinate change in the images taken 2 and 12 μm above the substrate–epilayer interface.

3. Results

Differential interference contrast (DIC) micrographs of the morphology of as-grown, 40 μm thick epilayers grown on three different substrates are shown in Figure 1. Hexagonal hillocks representing growth centers [13] and macro-steps.

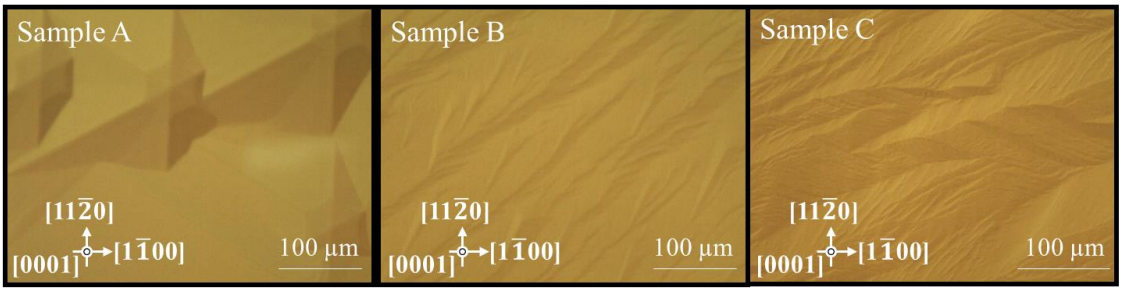

Figure 1. DIC optical micrographs of as-grown HVPE-GaN samples.

The (0002) and (10$\bar{1}$2) X-ray rocking curves (XRCs) of the samples before and after the growth are shown in Figure 2. The FWHM values of the peaks are listed in the upper right corners of the figures. Generally, Sample A showed narrower peaks, indicative of high crystalline quality, while samples B and C exhibited values indicative of a worse crystalline quality. Although the tilt values for the substrates and epilayers were similar in all cases (similar FWHM of the symmetric reflection), epilayers exhibited in the symmetric reflections a lower peak to tail intensity ratio. This was attributed to the broadening of the specular reflection intensity due to slight lattice undulations caused by inhomogeneous, growth-related imperfections [14]. The twist values for samples B and C showed a measurable improvement after the growth, and the multiple peaks indicate that the GaN substrates used here already contain several domains with different twists.

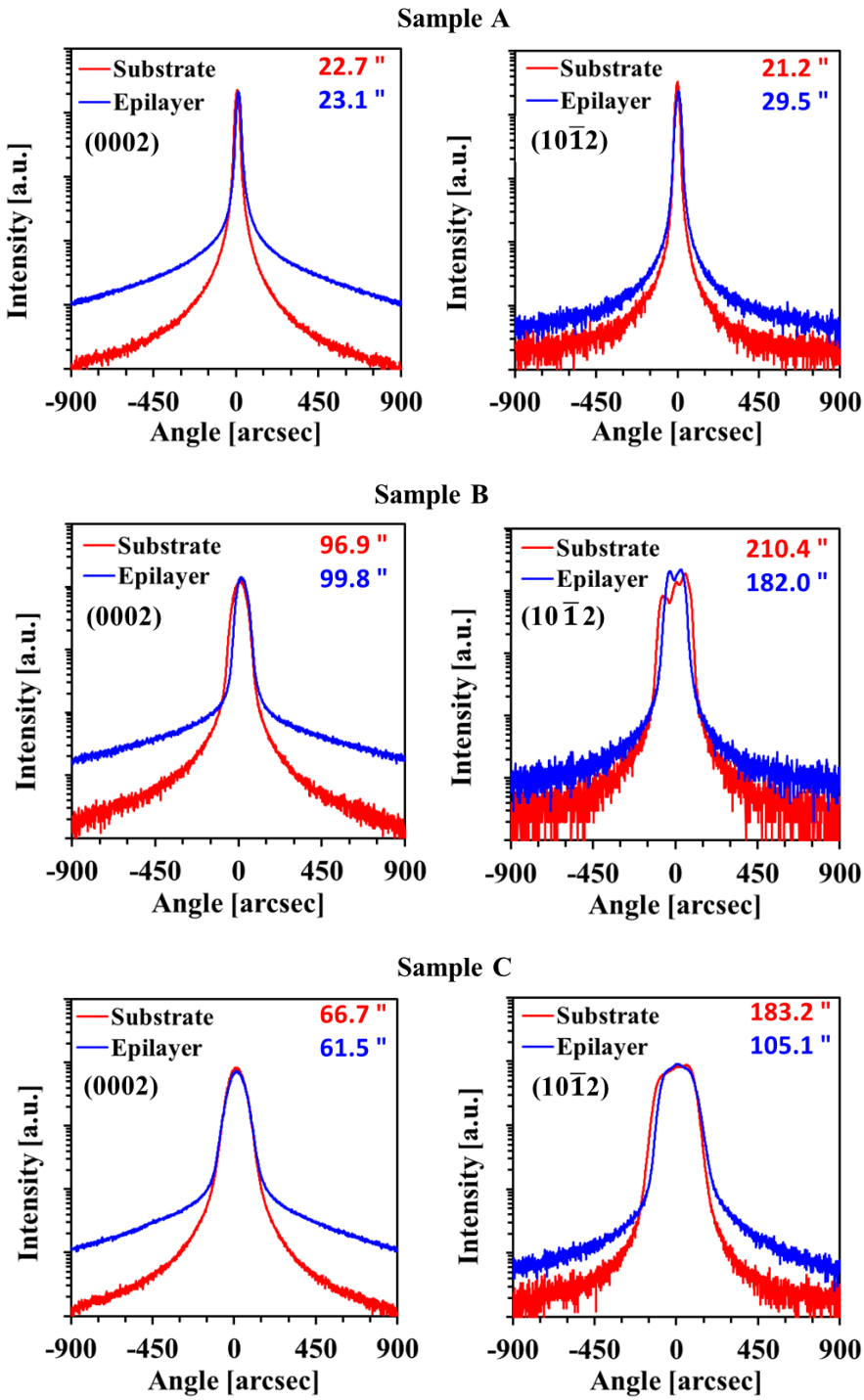

Figure 2. Logarithmic plots of (0002) and (10$\bar{1}$2) XRCs, evaluating the tilt and twist, respectively, before and after the growth.

Table II lists the measured lattice bow as radius of curvature, R_C, and the calculated strain and stress in two orthogonal directions ([1$\bar{1}$00] and [11$\bar{2}$0]) for all samples before and after the growth. The R_C values for the ammonothermally-grown substrates (Sample

A) were generally several hundred meters in either direction, while those of the HVPE-derived wafers were in the low teens (Sample B) or even single digits (Sample C), which is commensurate with the specified dislocation density (see Table I). It is important to point out that neither the sample B nor C can correctly reflect the-state-of-the-art 2-inch HVPE freestanding GaN wafer quality, the off angle variations for the 2-inch wafer can be decreased to below 0.1° [15]. Following the growth, all radii of curvature further decreased, indicating an accumulation of additional stress in the epilayers. A direct comparison of the change in the radii is not possible because the substrates have different layer thicknesses, and only the calculated stress can be compared. Based on the Stoney model [16], the in-plane strain was calculated to -1.9e-5 and -1.0e-5 in sample A, to 1.2e-5 and 6.3e-6 in sample B, and to 3.6e-5 in sample C. Using an Young's modulus of 300 GPa and Poisson ratio of 0.23 [17], it leads -8 and -4 MPa for sample A, +5 and +3 MPa for sample B, and +14 MPa for sample C. Furthermore, multiplying strain of each samples with ideal in-plane lattice constant of GaN of 0.318926 nm [18] results in "$a_{epilayer}$-$a_{substrate}$" of -6e-6 nm and -3e-6 nm for sample A, 4e-6 nm and 2e-6 nm for sample B, and 1e-5 nm for sample C, which are below the resolution of the XRD of about ±4e-5 nm in lattice constant a.

Table II. Measured radii of curvature and calculated strain and stress in the crystal along two orthogonal directions before and after the growth. Note: "-" designates convex bow or compressive strain and stress.

Direction	**Unit**	**Sample A**		**Sample B**		**Sample C**	
		[1$\bar{1}$00]	[11$\bar{2}$0]	[1$\bar{1}$00]	[11$\bar{2}$0]	[1$\bar{1}$00]	[11$\bar{2}$0]
substrate	[m]	-677	-246	13	14	5	5
epilayer	[m]	-50	-72	10	12	4	4
strain	[a.u.]	-1.9e-05	-1.0e-05	1.2e-05	6.3e-06	3.6e-05	3.6e-05
stress	[MPa]	-6.97	-3.70	4.40	2.27	12.97	12.97

Figure 3 shows a 3D view of dislocations in a volume 20 µm below to 20 µm above the homoepitaxial interface along with 2D slices taken 2 µm below (substrate) and 5 µm above (epilayer) the interface. A perusal of these images reveals several observations: (1) most dislocations propagate from the substrate into the epilayer, (2) many dislocations incline at the interface, and (3) new dislocations or even dislocation bundles form at the

homoepitaxial interface. Dislocation bundles were observed only on the HVPE-derived wafers and are likely a consequence of some surface residue from the polishing process.

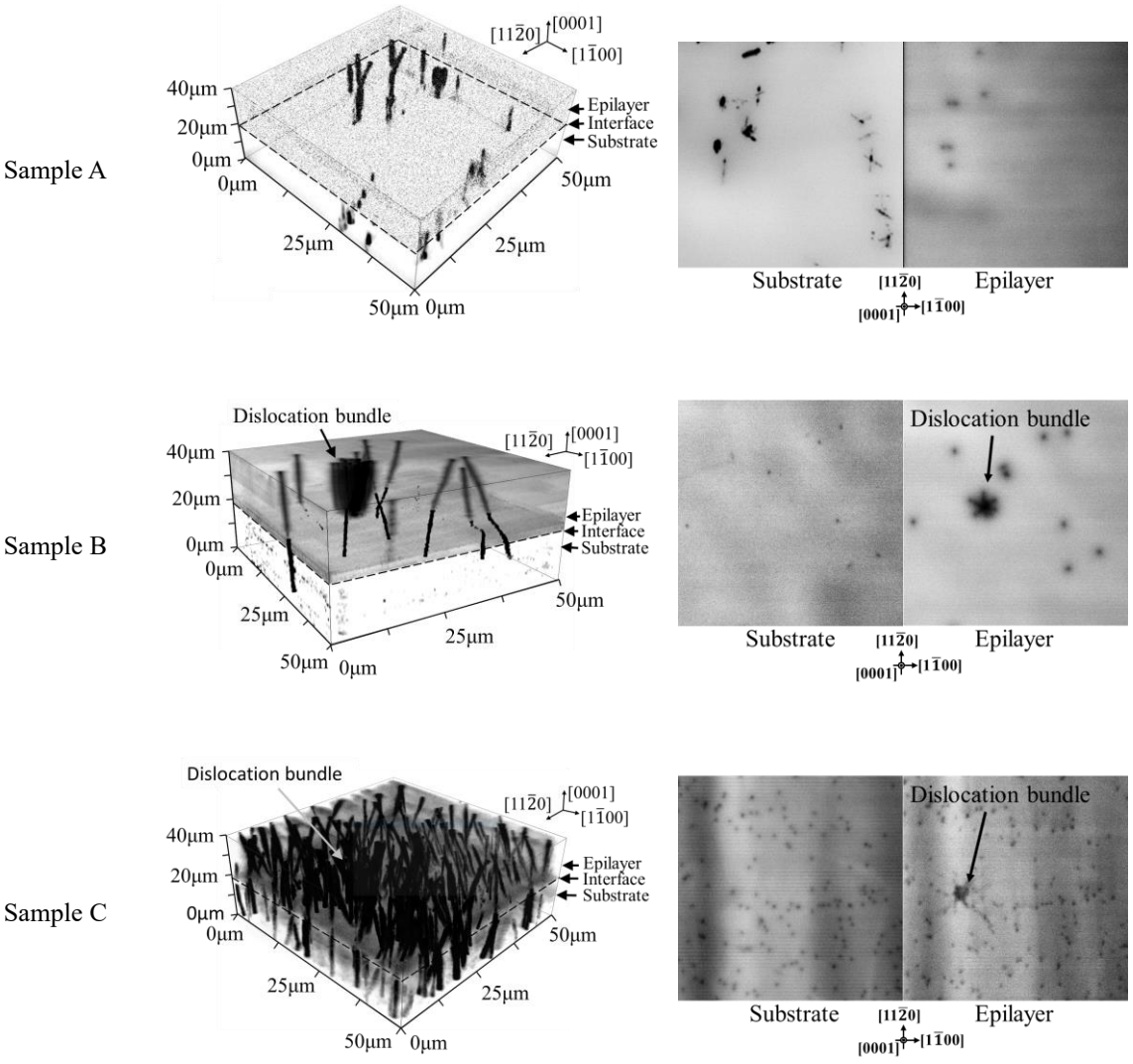

Figure 3. (left) 3D visualization of dislocation propagation through the interface; (right) 2D 2PPL images from the substrates and epilayers for Samples A through C.

The calculated values of the inclination angle, α, and direction of inclination are plotted in Figure 4. All individual dislocations visible in the 50x50 µm^2 were included for Samples A and B, while for Sample C, which has a much higher dislocation density, 25 dislocations were chosen at random for this analysis. Most dislocations in the GaN epilayer in Sample A propagated more or less perpendicular to the epilayer interface, as

indicated by the cluster of measurement points in the center of Figure 4, while a few were inclined about 10° from the c-direction. The α values measured in Samples B and C were mostly around 10°, although inclination as high as 20° was observed. Interestingly, the inclination direction seemed to be more or less random, as can be seen in Figure 4. This phenomenon is also observed in Si doped GaN layers grown by metalorganic chemical vapor deposition [19]. But in this experiment, all the samples were grown in the same reactor at the same time, the Si doping level for all the epilayer should also be the same. The directional dependence of inclination, the result from Sample A may be statistically irrelevant.

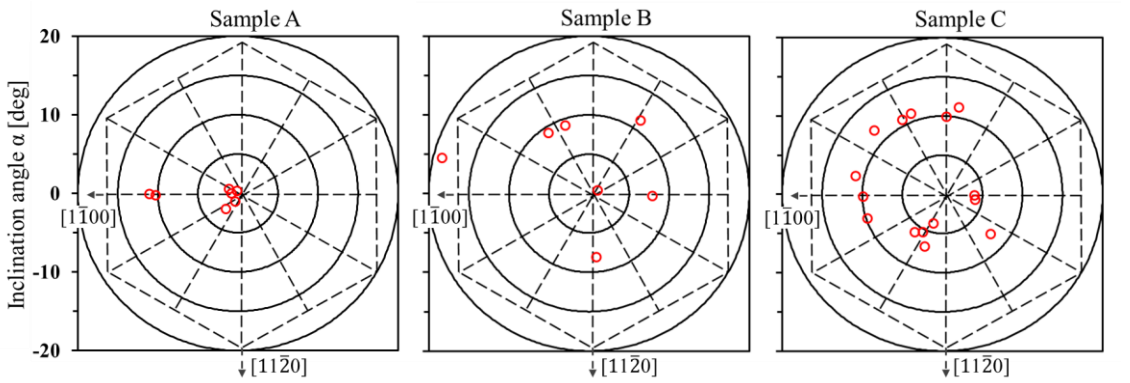

Figure 4 Polar plots of dislocation inclination for the 3 samples. Each circle represents 5°; dashed hexagon illustrates the crystallographic directions.

4. Discussion

In general, wafer bow in homoepitaxy can be influenced by: (1) slight lattice mismatch between the substrate and overgrowth due to different point defect densities, (2) change in dislocation density and the associated strain energy due to dislocation inclination or generation of new dislocations, or (3) various edge effects ranging from spurious growth on the edges or formation of facets. For the first two cases, simple models exist to evaluate additional stress and associated bow while the last case is related to some challenge in controlling the growth process and requires a system-specific solution.

The lattice parameters of the wafers and epilayers were too close and were below the resolution of the XRD, which rendered the contribution from the point-defect-related

mismatch insignificant. The mechanism behind the relaxation of compressive stresses can be further explained by a model described in Ref. [11], in which the tensile stress is proportional to the threading dislocation density and average threading dislocation inclination angle. The calculated tensile stresses for Sample A to C were 0.16 MPa, 11.52 MPa and 20.22 MPa, which deviate from the calculated stress listed in Table II. An extra constant compressive stress about -7 MPa by some spurious edge effect may help to explain the deviation. The overall stress for Sample A to C can then be calculated to -6.84 MPa, 4.52 MPa and 13.22 MPa, and these values are close to those listed in Table II.

This calculation can only provide an idea to explain the different stresses observed in these three different samples. The tensile stress calculation with the model may slightly deviate from the actual value because the inclination of dislocation in the model is only in $[1\bar{1}00]$ direction and only misfit segments (only inclined TDs, only climb) contribute to the total stress. The edge effect of these samples has not been studied. One of the detailed studies on the edge effect can be found in Ref. [20].

5. Conclusions

Lattice bow is a crucial wafer parameter as it determines the variation of the offcut across the surface. For the growth of epi-structures and fabrication of devices, the wafer surface must be offcut uniformly with an accuracy of one to two tenths of a degree in a specific crystallographic direction, which produces specific step structure on the wafer's surface that controls surface morphology, composition of ternary alloys, and uniformity of doping. Note that an acceptable offcut variation across the wafer of 0.1° pegs the minimum acceptable radius of curvature for a 2-inch wafer to more than 30 m, which is far above the specifications of the HVPE GaN wafers on the market. To make matters worse, and as seen in this study, the initial lattice bow only worsens with further growth of thick layers needed in vertical power devices, thus, flattening of the regrown surfaces via polishing would result in an increased offcut variation across the wafer and ultimately to lower device uniformity and yield.

Although the bow after homoepitaxial growth worsened also for the ammonothermally grown substrates (Sample A), the resulting radius of curvature still enabled uniform properties across at least a 4-inch wafer. Since the dislocation density in the epilayers was similar to that of the substrates, the measured bow was likely a consequence of some edge effects, which can be easily mitigated by the growth.

Acknowledgements

This work was supported by MEXT "Research and development of next-generation semiconductor to realize energy-saving society" Program Grant Number JPJ005357. The authors would like to thank Professor Akira Usui of Japan Science and Technology Agency and Doctor Eberhard Richter of Ferdinand-Braun-Institute for fruitful discussions.

References

[1] L.M. Tolbert, Power Electronics for Distributed Energy Systems and Transmission and Distribution Applications: Assessing the Technical Needs for Utility Applications, Oak Ridge National Lab. (ORNL), Oak Ridge, TN (United States), 2005. https://doi.org/10.2172/885985.

[2] B.J. Baliga, Gallium nitride devices for power electronic applications, Semicond. Sci. Technol. 28 (2013) 074011. https://doi.org/10.1088/0268-1242/28/7/074011.

[3] R.P. Tompkins, M.R. Khan, R. Green, K.A. Jones, J.H. Leach, IVT measurements of GaN power Schottky diodes with drift layers grown by HVPE on HVPE GaN substrates, J Mater Sci: Mater Electron. 27 (2016) 6108–6114. https://doi.org/10.1007/s10854-016-4536-z.

[4] H. Fujikura, K. Hayashi, F. Horikiri, Y. Narita, T. Konno, T. Yoshida, H. Ohta, T. Mishima, Elimination of macrostep-induced current flow nonuniformity in vertical GaN PN diode using carbon-free drift layer grown by hydride vapor phase epitaxy, Appl. Phys. Express. 11 (2018) 045502. https://doi.org/10.7567/APEX.11.045502.

[5] H. Nie, Q. Diduck, B. Alvarez, A.P. Edwards, B.M. Kayes, M. Zhang, G. Ye, T. Prunty, D. Bour, I.C. Kizilyalli, 1.5-kV and 2.2-mΩ-cm2 Vertical GaN Transistors on Bulk-GaN Substrates, IEEE Electron Device Letters. 35 (2014) 939–941. https://doi.org/10.1109/LED.2014.2339197.

[6] S. Chowdhury, Vertical Gallium Nitride Technology, in: M. Meneghini, G. Meneghesso, E. Zanoni (Eds.), Power GaN Devices: Materials, Applications and Reliability, Springer International Publishing, Cham, 2017: pp. 101–121. https://doi.org/10.1007/978-3-319-43199-4_5.

[7] R.P. Tompkins, J.R. Smith, K.W. Kirchner, K.A. Jones, J.H. Leach, K. Udwary, E. Preble, P. Suvarna, J.M. Leathersich, F. Shahedipour-Sandvik, GaN Power Schottky Diodes with Drift Layers Grown on Four Substrates, Journal of Elec Materi. 43 (2014) 850–856. https://doi.org/10.1007/s11664-014-3021-9.

[8] H. Fujikura, T. Konno, T. Yoshida, F. Horikiri, Hydride-vapor-phase epitaxial growth of highly pure GaN layers with smooth as-grown surfaces on freestanding GaN substrates, Jpn. J. Appl. Phys. 56 (2017) 085503. https://doi.org/10.7567/JJAP.56.085503.

[9] P. Kruszewski, P. Prystawko, M. Grabowski, T. Sochacki, A. Sidor, M. Bockowski, J. Jasinski, L. Lukasiak, R. Kisiel, M. Leszczynski, Electrical properties of vertical GaN Schottky diodes on Ammono-GaN substrate, Materials Science in Semiconductor Processing. 96 (2019) 132–136. https://doi.org/10.1016/j.mssp.2019.02.037.

[10] I. Bryan, Z. Bryan, S. Mita, A. Rice, J. Tweedie, R. Collazo, Z. Sitar, Surface kinetics in AlN growth: A universal model for the control of surface morphology in III-nitrides, Journal of Crystal Growth. 438 (2016) 81–89. https://doi.org/10.1016/j.jcrysgro.2015.12.022.

[11] H.M. Foronda, A.E. Romanov, E.C. Young, C.A. Robertson, G.E. Beltz, J.S. Speck, Curvature and bow of bulk GaN substrates, Journal of Applied Physics. 120 (2016) 035104. https://doi.org/10.1063/1.4959073.

[12] T. Tanikawa, K. Ohnishi, M. Kanoh, T. Mukai, T. Matsuoka, Three-dimensional imaging of threading dislocations in GaN crystals using two-photon excitation photoluminescence, Appl. Phys. Express. 11 (2018) 031004. https://doi.org/10.7567/APEX.11.031004.

[13] T. Sochacki, M. Amilusik, B. Lucznik, M. Fijalkowski, J.L. Weyher, G. Nowak, B. Sadovyi, G. Kamler, R. Kucharski, M. Iwinska, I. Grzegory, M. Bockowski, HVPE-GaN growth on misoriented ammonothermal GaN seeds, Journal of Crystal Growth. 403 (2014) 32–37. https://doi.org/10.1016/j.jcrysgro.2014.06.020.

[14] P.F. Fewster, Estimating the structure factors in X-ray diffraction, Acta Cryst A. 74 (2018) 481–498. https://doi.org/10.1107/S2053273318007593.

[15] H. FUJIKURA, T. INOUE, T. KITAMURA, T. KONNO, T. SUZUKI, T. FUJIMOTO, T. YOSHIDA, M. SHIBATA, T. SAITO, Development of GaN Single-Crystal Substrates, SCIOCS Co., Ltd., 2018.

[16] G.G. Stoney, C.A. Parsons, The tension of metallic films deposited by electrolysis, Proceedings of the Royal Society of London. 82 (1909) 172–175. https://doi.org/10.1098/rspa.1909.0021.

[17] H. Qin, X. Luan, C. Feng, D. Yang, G. Zhang, Mechanical, thermodynamic and electronic properties of wurtzite and zinc-blende GaN crystals, Materials. 10 (2017) 1419.

[18] V. Darakchieva, B. Monemar, A. Usui, M. Saenger, M. Schubert, Lattice parameters of bulk GaN fabricated by halide vapor phase epitaxy, Journal of Crystal Growth. 310 (2008) 959–965. https://doi.org/10.1016/j.jcrysgro.2007.11.130.

[19] J. Weinrich, A. Mogilatenko, F. Brunner, C.T. Koch, M. Weyers, Extra half-plane shortening of dislocations as an origin of tensile strain in Si-doped (Al)GaN, Journal of Applied Physics. 126 (2019) 085701. https://doi.org/10.1063/1.5111664.

[20] M. Amilusik, D. Wlodarczyk, A. Suchocki, M. Bockowski, Micro-Raman studies of strain in bulk GaN crystals grown by hydride vapor phase epitaxy on ammonothermal GaN seeds, Jpn. J. Appl. Phys. 58 (2019) SCCB32. https://doi.org/10.7567/1347-4065/ab1390.